PAPER

3D nanostructure reconstruction based on the SEM imaging principle, and applications

To cite this article: Fu-Yun Zhu *et al* 2014 *Nanotechnology* **25** 185705

View the article online for updates and enhancements.

Related content

- Characterization of surface topography by SEM and SFM: problems and solutions
- Critical factors in SEM 3D stereo microscopy
- Effect of black silicon disordered structures distribution on its wideband reduced reflectance

Recent citations

- In situ characterization of nanoscale strains in loaded whole joints via synchrotron X-ray tomography
Kamel Madi *et al*
- Polarization Modulation of Terahertz Wave by Femtosecond Laser Additive Manufactured Tin Grating
Yao Li *et al*
- Research Update: Electron beam-based metrology after CMOS
J. A. Liddle *et al*

239th ECS Meeting
with the 18th International Meeting on Chemical Sensors (IMCS)
ABSTRACT DEADLINE: DECEMBER 4, 2020

May 30-June 3, 2021
SUBMIT NOW

This content was downloaded from IP address 117.131.219.8 on 17/11/2020 at 11:26

IOP Publishing

Nanotechnology

Nanotechnology 25 (2014) 185705 (10pp)

doi:10.1088/0957-4484/25/18/185705

3D nanostructure reconstruction based on the SEM imaging principle, and applications

Fu-Yun Zhu[1], Qi-Qi Wang[2], Xiao-Sheng Zhang[1], Wei Hu[1], Xin Zhao[2] and Hai-Xia Zhang[1]

[1] National Key Laboratory of Science and Technology on Micro/Nano Fabrication, Institute of Microelectronics, Peking University, Beijing 100871, People's Republic of China
[2] Institute of Robotics and Automatic Information System, Nankai University, Tianjin 300071, People's Republic of China

E-mail: zhang-alice@pku.edu.cn (H-X Zhang)

Received 14 October 2013, revised 30 December 2013
Accepted for publication 14 January 2014
Published 16 April 2014

Abstract

This paper addresses a novel 3D reconstruction method for nanostructures based on the scanning electron microscopy (SEM) imaging principle. In this method, the shape from shading (SFS) technique is employed, to analyze the gray-scale information of a single top-view SEM image which contains all the visible surface information, and finally to reconstruct the 3D surface morphology. It offers not only unobstructed observation from various angles but also the exact physical dimensions of nanostructures. A convenient and commercially available tool (NanoViewer) is developed based on this method for nanostructure analysis and characterization of properties. The reconstruction result coincides well with the SEM nanostructure image and is verified in different ways. With the extracted structure information, subsequent research of the nanostructure can be carried out, such as roughness analysis, optimizing properties by structure improvement and performance simulation with a reconstruction model. Efficient, practical and non-destructive, the method will become a powerful tool for nanostructure surface observation and characterization.

Keywords: 3D reconstruction, SEM imaging principle, nanostructures, shape from shading, statistical analysis

(Some figures may appear in colour only in the online journal)

1. Introduction

Since the 2000s, NEMS (nano electro-mechanical systems), as a joint branch of both nanotechnology and MEMS (micro electro-mechanical systems), has taken advantage of the unique mechanical and electrical properties of nanoscale structures to achieve functions of perception, analysis and even execution. Together with nanotechnology, NEMS has achieved important research significance and seen application in many fields such as high sensitivity devices, nano energy, biomedical and micro optics [1–4], etc. It has become an important paving stone of interdisciplinary science which will be of benefit to society.

Obviously, the performance of NEMS devices is determined by their structures to a large extent—carbon nanotube, nanowire and so on [5, 6]. Admittedly, their favorable properties strongly depend on the nanostructure morphology, which is not completely regular [7]. Normally, it is hard to achieve controllability and repeatability of some nanostructures either in the lab or in mass production; most of the nanostructures cannot be measured directly. The most convenient approach for researchers is to take scanning electron microscopy (SEM) images of structures. However, an SEM image is two-dimensional (2D), and cannot provide enough details for statistical regularity of structures. Therefore, how to obtain more reliable information regarding nanostructures is a serious problem.

In fact, there are several difficulties for getting comprehensive information regarding nanostructures, for example some nanostructures are immeasurable, some measurements

 © 2014 IOP Publishing Ltd Printed in the UK

are inefficient and inaccurate, because they are often affected by structure sheltering and perspective effects, and some measurements have to damage samples to reveal their cross section profiles [8]. Thus, researchers have turned their attention to SEM-based three-dimensional (3D) reconstruction technology [9–23], which is a powerful computer technology with the advantage over direct measurement of offering unobstructed observation from various angles as well as the exact physical dimensions. It has attracted much attention and has been researched extensively. 3D reconstruction is especially important for special conditions—for instance, some specimens no longer exist but their SEM images can be utilized to reconstruct their surface structure.

At present, there are three main kinds of 3D reconstruction methods, categorized according to their different applicative structures. The first is the reconstruction of serial sections [9], which focuses on internal structures, such as of biological samples or porous electrodes. To achieve a series of images, a dual-beam focused ion beam/scanning electron microscopy (FIB/SEM) system [10–12] can be used. But the procedure is destructive to samples and the reconstruction resolution is restricted by the thickness of milled layers with FIB. The second method is the stereo photogrammetry technique, using more than two images from different perspectives [13–16]. However, it has difficulty in both corresponding point matching and the reconstruction algorithm. The third method is the quasi-planar stereovision technique [17–23]. A stereo pair is typically obtained by tilting the sample by a few degrees. This has the same problems as stereo photogrammetry, but it is a little simpler and is correspondingly suitable for simpler structures. For all the above reconstruction methods, a common problem is the inconvenience, especially for some simple nanostructures for which there is no interest in the internal structure. This can involve not only a waste of money and time, but also a lot of unnecessary work.

In order to solve the above problems, a novel convenient and non-destructive 3D reconstruction method based on a single image is provided in this paper. It needs only one top-view SEM image to quantify the surface morphology of nanostructures in 3D and offers several practical characterizations and applications.

2. Reconstruction theory

Contrast plays an important role in the process of human visual perception. People can restore 3D information accurately from shading through the eye and the brain. SFS (shape from shading) technology uses the gray-scale value of corresponding points from an image of a surface to reconstruct the 3D surface morphology. This technology was first put forward by Horn for reconstruction of the lunar surface in 1970 [24]. As only one single 2D image is required, it has been very popular in the computer vision field and has very attractive application prospects in various fields [25–27], especially in SEM-based 3D reconstruction [28–31].

In the microelectronics field, almost all the structures exist in a microcosmos and they are commonly observed by SEM equipment. This paper employs the SFS method to analyze the gray-scale information of SEM images and to reconstruct the surface morphology of nanostructures.

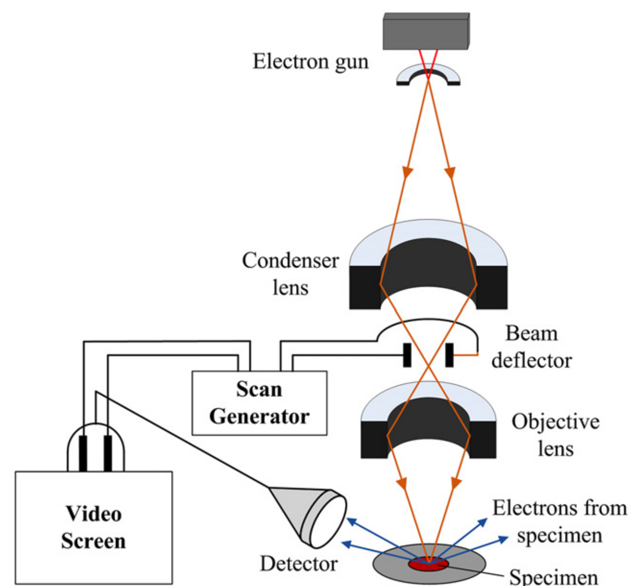

Figure 1. Schematic diagram of the SEM working principle [32].

2.1. The SEM imaging principle

Figure 1 shows a schematic diagram of the SEM working principle [32]. First, an electron gun emits electrons. Under the action of acceleration voltage, the electrons pass through the condenser lens and the objective lens, and form an electron beam with a diameter of just a few nanometers. Then electron signals are generated by the beam–specimen interaction processes when the electron beam bombards the specimen surface. While the electron beam scans over the specimen surface rectilinearly, the electron signals are detected synchronously by the detector and converted into the brightness of corresponding points according to the amount of detected electrons and then displayed on a video screen, thus forming the corresponding electron image.

Generally, there will be various electron signals emitted by the interaction between the incident electron beam and the specimen surface, including those of Auger electrons, characteristic x-rays, transmission electrons, absorption electrons, backscattered electrons (BSEs), secondary electrons (SEs) and so on [32, 33], as shown in figure 2.

Among them, the Auger electrons and characteristic x-rays can be used in a spectrometer to analyze the chemical composition of a specimen. Transmission electrons are often used in a transmission electron microscope (TEM) to observe morphology details because of the very high resolution. Absorption electrons and BSEs both collect chemical composition information. As one might imagine, the more BSEs that are produced, the fewer absorption electrons are left, resulting in images of opposite contrast.

For morphology imaging, there are two main kinds of detection principle: SE and BSE. However, the generation of BSE is more related to chemical elements, and its resolution for morphology is too low, so it is rarely used for morphology characterization. Compared to BSE, SE is usually preferred since it provides topographies with an optimal signal-to-noise ratio and eventually with very high resolution. Thus SE

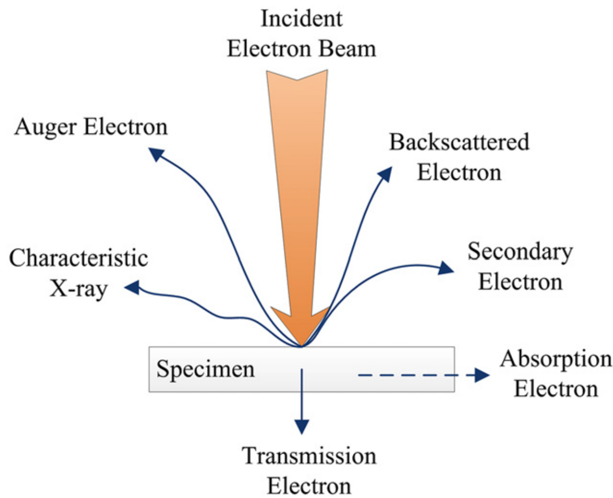

Figure 2. Generation of electron signals emitted by the interaction between the incident electron beam and the specimen surface [32, 33]. Reprinted with permission from [4]. Copyright 2013 IEEE.

imaging is widely used in SEM equipment to characterize surface morphology [34].

2.2. The secondary electron imaging model

SFS technology can be regarded as an inverse process of imaging. In order to obtain the exact solution of an SFS problem, the formation mechanism of an image has to be identified. The contrast is the 3D clue remaining in the 2D SEM image which can be extracted to rebuild the 3D vector field. The key point is to establish an appropriate imaging model which can describe well the relationship between the electron signal intensities of each point on the surface and their corresponding gray-scale values in the image.

The quality of an SE image is related to the following factors: the accelerating voltage, the spot size, the working distance, the relative position of the specimen to the SE detector, and the morphology and material of the specimen [34, 35]. It is very difficult to quantify all of these. However, some factors can be ignored in certain cases. Here an ideal SE imaging model is set up based on the following assumptions: the specimen has only one chemical element; it has a relatively simple structure with small dimensions; the working distance is far larger than the specimen dimensions; all of the generated SEs can be collected by the SE detector. In this model, what should be taken into consideration is just the generation mechanism of the SE process.

It is worth noting that an SE is able to escape from a specimen only when it is less than 10 nm from the surface [33] and this is also one of the main reasons for the high resolution of the SE image [34]. In figure 3, the thickness of this superficial layer is marked as L. When the incident electron beam is perpendicular to the specimen surface ($\theta = 0$), SEs have the minimum escape area and correspondingly the least output. When the incident angle $\theta > 0$, the escape area of SEs increases and so does output. Thus the generation law of SEs can be described as follows: the generation number of SEs on the specimen surface (G) is inversely proportional to the cosine of the angle between the incident electron beam and the normal to the specimen surface (θ),

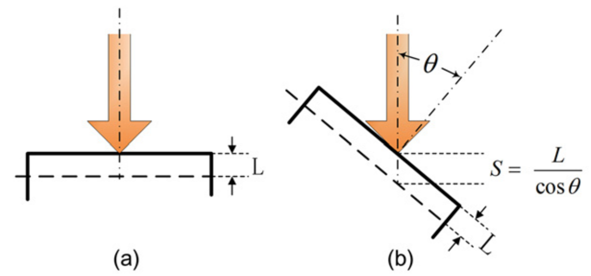

Figure 3. Effect of the incident angle between the incident electron beam and the normal to the specimen surface on the escape path of secondary electrons. (a) $\theta = 0°$, (b) $\theta > 0°$, $\theta \in (0, \pi/2)$. Reprinted with permission from [4]. Copyright 2013 IEEE.

$$G = k/\cos\theta. \quad (1)$$

Here, k is the generation coefficient of SEs. Obviously, the larger θ is, the more SEs will be energized, indicating that the SE process is very sensitive to specimen surface morphology.

Given that the gray scale of the SE image is determined by the amount of SEs, the following formula can be deduced:

$$E = k'/\cos\theta. \quad (2)$$

Here, E is the gray scale of each pixel in the SEM image, k' is a rectifiable constant which is determined by the gray scale of the darkest point in each image, and θ is the angle between the incident electron beam and the normal of the specimen surface, $\theta \in [0, \pi/2)$.

2.3. Formula derivation and algorithm solution

According to the analytical geometry, the cosine of θ can be expressed as

$$\cos\theta = \frac{p_s p(x, y) + q_s q(x, y) + 1}{\sqrt{p_s^2 + q_s^2 + 1}\sqrt{p(x, y)^2 + q(x, y)^2 + 1}}, \quad (3)$$

where $(p_s, q_s, -1)$ is the direction vector of the incident electron beam and $(p(x, y), q(x, y), -1)$ is the normal vector of the specimen surface corresponding to the pixel (x, y). The minimum unit in an SEM image is one pixel, so (4) and (5) can be used as approximations for the gradients along the x and y directions, i.e. $p(x, y)$ and $q(x, y)$; $z(x, y)$ is the height of the surface structure at (x, y).

$$p(x, y) = \frac{\partial z}{\partial x} = Z(x, y) - Z(x - 1, y) \quad (4)$$

$$q(x, y) = \frac{\partial z}{\partial y} = Z(x, y) - Z(x, y - 1). \quad (5)$$

From (2) to (5), the calculated gray scale R at (x, y) can be expressed as a function of $p(x, y)$ and $q(x, y)$,

$$R_\theta = R(p(x, y), q(x, y)). \quad (6)$$

However, equation (6) is an ill-posed equation which has no unique solution. In order to eliminate the ill-posed problem, the smoothness constraint as shown in equation (7) is introduced,

$$\iint (p_x^2 + p_y^2 + q_x^2 + q_y^2)\,\mathrm{d}x\,\mathrm{d}y. \quad (7)$$

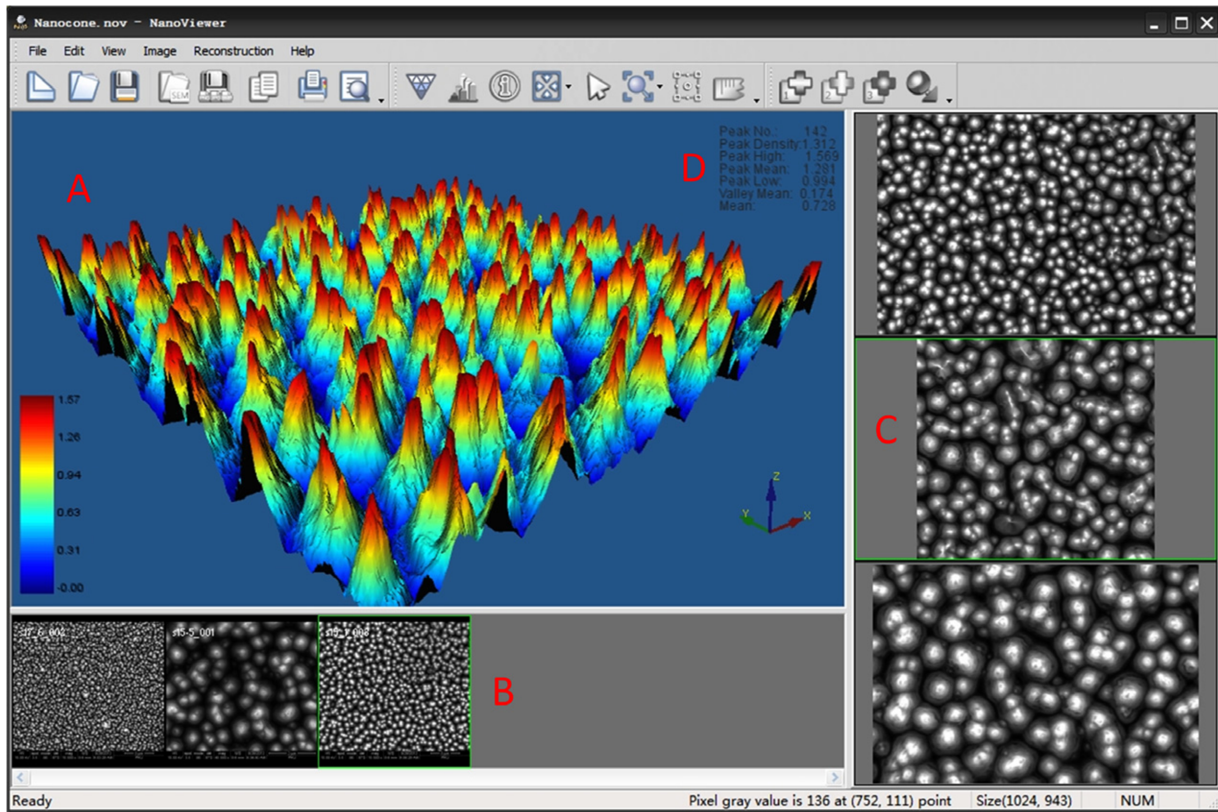

Figure 4. Interface diagram of NanoViewer software. (A) Display window of SEM image and reconstruction result; (B) list of input SEM images; (C) selected areas to reconstruct; (D) statistical analysis result of reconstructed nanostructures.

Here, p_x, p_y, q_x and q_y are the partial derivatives of $p(x, y)$ and $q(x, y)$ along the x and y directions, respectively. This guarantees that the surface is continuous and smooth in every direction.

Finally, by introducing a coefficient λ, the final irradiance equation [36] can be written as

$$\iint \left[(E(x, y) - R_\theta)^2 + \lambda(p_x^2 + p_y^2 + q_x^2 + q_y^2) \right] \mathrm{d}x\, \mathrm{d}y, \qquad (8)$$

where $E(x, y)$ is the gray scale at pixel (x, y) in the SEM image and λ is a customized coefficient which represents the effect level of the smooth constraint condition. Equation (8) has a unique solution.

The existing SFS algorithm can be divided into four categories: minimization approaches, propagation approaches, local approaches and linear approaches [37]. Among them, minimization approaches have high calculation precision and are the most robust. However they are significantly slower than other approaches, because for the minimization approaches, time depends not only on the size of the input image, but also varies from scene to scene. However, this problem can be ignored nowadays owing to the availability of high-speed computers. Therefore minimization approaches are most commonly used, and they were adopted in this work [37, 38].

Finally, the optimal solution will be obtained once equation (8) reaches the minimum. After automatic computer solution and 3D reconstruction, the height and angle value of each pixel can be obtained and finally used to reconstruct the surface structures.

3. Results and analysis

3.1. Reconstruction tool development

The 3D reconstruction method in this paper has been developed into the commercial software 'NanoViewer' by the Intellisense Corporation [39]. The software interface diagram is shown in figure 4. Besides the basic menu bar and toolbar, there are four main regions in the interface. (A) Is the display window of SEM images and reconstruction results which can be switched between; (B) is the list of input SEM images; (C) shows the selected areas to reconstruct for each SEM image; (D) is the statistical analysis result of reconstructed nanostructures.

With this software, users can select any area in an SEM image to reconstruct at will. The reconstruction result can offer not only unobstructed view observation, but also the nanostructure dimension information. The size of nanostructures is calculated based on the sampling in the SEM image.

This tool also has several auxiliary functions such as measuring distance, zooming in/out, exporting files in different formats, and so on.

3.2. Reconstruction results

In this paper, black silicon samples were taken as examples to show the effect of this 3D reconstruction method. The samples were fabricated by an improved deep reactive ion etching (DRIE) process which is maskless, large-area, low-cost, controllable and highly efficient [8, 40, 41]. Compared

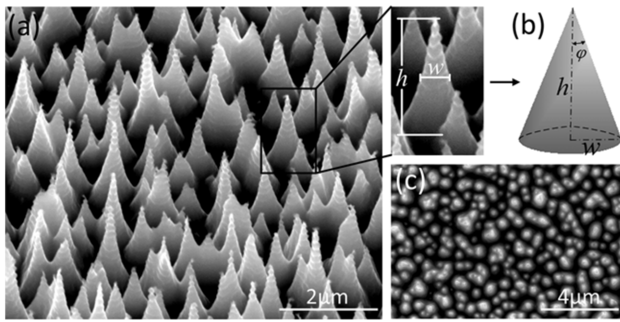

Figure 5. SEM of typical nanocone structures formed by improved DRIE. (a) Side-view SEM image (all the side-view SEM images in this paper were taken at 45° tilt angle); (b) a standard cone model for definition of nanocone structure parameters; (c) top-view SEM image of black silicon.

to conventional DRIE, nanoparticles appear after several etching/passivation cycles during the improved DRIE process, which works by optimizing the process parameters. Generally, the generation of nanoparticles is caused by the residue of the polymeric layer deposited during the passivation period working as nanomasks during the following DRIE process. With this process, a low reflective silicon surface with regular nanocone structures is achieved [42, 43].

Typical black silicon with a nanocone structure is shown in figure 5(a) and can be seen as equivalent to the cone model in figure 5(b), which makes the definition of structure parameters clear. Specifically, the width of the nanocone is defined as FWHM (full-width at half maximum) [44] which is numerically equal to the bottom radius (w) in the standard cone model. As there is only the Si element in the black silicon sample and its structure dimension is relatively small, the reconstruction method is applicative. Figure 5(c) shows a top-view SEM image of black silicon which will be used to reconstruct the 3D structure, for two reasons: first, the gradient of surface structure obtained from the top view is the real gradient without deformation; second, all the black silicon surface structure can be shown in a top-view image with no sheltering from other structures.

Figure 6 shows the reconstruction results of the black silicon sample. The side-view SEM images were taken from four different views at every 90°. Two distinctly larger silicon cones as marked in the top-view SEM image in figure 6(a) were taken as references.

The comparison between reconstruction results and SEM images in figure 6 shows that all the morphological features of the black silicon sample, even the details which cannot be seen clearly in the SEM image, have been well reconstructed. It can be observed clearly from the different views that the distribution of reconstruction structures fits the SEM image well. In particular, the comparison of structures in the same position between the reconstruction result and the SEM image shows that they match well for both structure shape and structure size. The reconstruction details are shown in figure 6(b), containing only a few nanostructures. The reconstruction result is good enough to see the slope changes between nanostructures on the bottom, which cannot be seen in the SEM image.

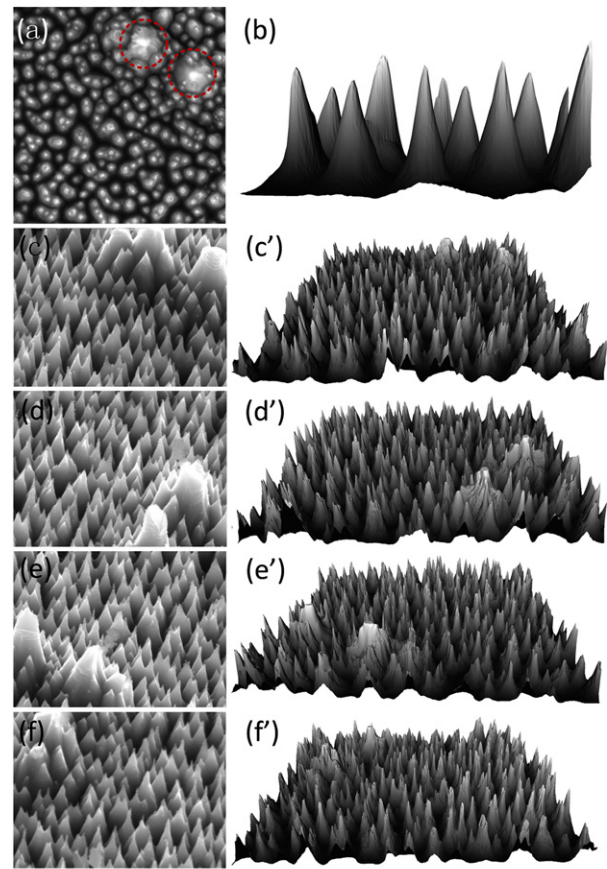

Figure 6. Comparison between SEM images and 3D reconstruction results of black silicon sample; (a) top-view SEM image with reference structures marked by red frames; (b) reconstruction result of nanocone details; ((c), (c′))–((f), (f′)) comparison from different views. (The side-view SEM images were taken from four different views at every 90°.)

Because the complexity of the SEM imaging and errors that cannot be avoided in experiment will both affect the reconstruction result, we also performed several experiments on synthetic gray-scale images which were simulated in open GL by introducing the SEM imaging principle, including an ideal sphere and an ideal cone, expecting to provide an ideal initial condition for evaluating the performance of the proposed method. As shown in figure 7, both the sphere and the cone have perfect reconstruction results. At the same time, as the gray-scale image of the cone has fewer pixels than that of the sphere, its reconstructed surface is rougher with less detail, indicating the importance of image resolution.

In order to compare the reconstruction result of the real SEM image with that of the synthetic image intuitively, we deliberately selected a clear SEM area of a single silicon cone to reconstruct. As can be seen from figure 8(a), the gray-level distribution of the top-view image of the silicon cone was basically the same as in figure 7(c), dimming gradually from the center to the edge. Because there are other structures around this silicon cone, the gray level at the edge changes gently and continuously. The reconstructed top-view image (figure 8(b)) keeps the same intensity distribution as its original gray-scale image. In figure 8(c), the reconstructed side-view nanocone

Table 1. Statistical structure parameters of 3D reconstruction results of black silicon samples.

Sample	Height (μm) Mean value	SD	Distribution type	Significance level	Width (μm) Mean value	SD	Distribution type	Significance level	Density (μm^{-2})	Aspect ratio
I	2.30	0.201	Uniform	0.3870	0.366	0.031	Uniform	0.5000	3.84	6.3
II	1.30	0.113	Normal	0.3950	0.204	0.017	Normal	0.5000	6.57	6.4

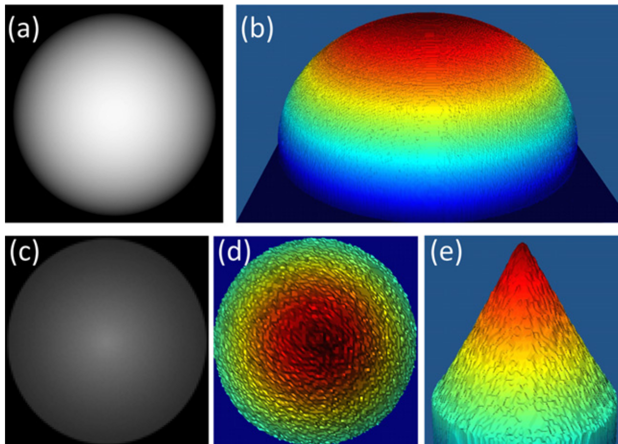

Figure 7. Reconstruction of synthetic images; (a) and (b) an ideal sphere, (c)–(e) an ideal cone.

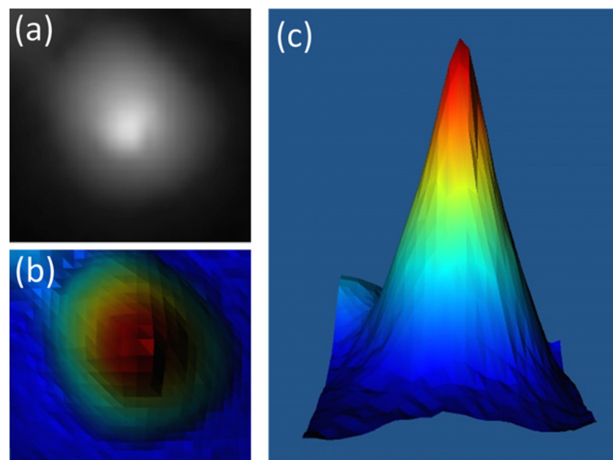

Figure 8. Reconstruction of a single silicon cone; (a) selected area in SEM image; (b) reconstruction result of top view; (c) reconstruction result of side view.

looks quite good. However, as it has even fewer pixels than figure 7(c), its reconstructed surface element is very large and it is not smooth enough at the joint of the surface elements. All of these experiment results show the validity of this 3D reconstruction method.

3.3. Data extraction and statistical analysis

Statistical analysis is carried out automatically after getting the shape parameters from the reconstruction results. The statistical information of two black silicon samples with different distribution types are listed in table 1.

In figure 9, the frequency distribution histograms of shape parameters demonstrate that each black silicon sample obeys either uniform distribution or normal distribution for both height and width. Their significance levels are far larger than 0.05, indicating that the distribution types are reliable. Mean value represents the structure size of the sample while standard deviation (SD) demonstrates that the uniformity is very good in the same sample. Besides height, width, density and semi-apex angle, which can be extracted directly by reconstruction, other structure parameters such as aspect ratio, periodicity, and occupied ratio can be achieved easily after a few simple calculations or conversion.

In addition, different formats of 3D models can be exported from NanoViewer, including IV, WRL, DXF, STL, etc. These model files provide convenience for continuing research with other tools, such as 3D MAX, Open Inventor, AutoCAD, PROE, and so on. For a large-area sample, a standard cone model, as shown in figure 5(c), can be established with extracted mean shape parameters for further research.

3.4. Verification of reconstruction results

The comparisons between reconstruction results and SEM images have shown very good coincidence as described above. The 3D reconstruction results have also been verified by comparing them to the actual measured values of the shape parameters of black silicon samples. After taking the cross-sectional view SEM image, the parameters including height, width and semi-apex angle are measured accurately from all the clear and complete nanocones as illustrated in figure 10. Then the mean values of these measured parameters are calculated and compared to the mean values extracted from the reconstruction result, as listed in table 1. The results show that these two kinds of mean values of the same sample are almost equivalent to each other, proving the rationality and validity of this method.

Figure 11 shows the verification of reconstruction results of the synthetic images in figure 7. In figure 11(a), the horizontal diameter D and vertical radius R of the reconstructed sphere follow the relationship $D = 2R$, proving that the reconstructed structure is a complete standard sphere. For the cone, the apex angle was reconstructed without variation, indicating that the reconstruction result is completely consistent with the real structure.

4. Applications and discussion

4.1. Roughness analysis

In surface characterization, roughness is a vital parameter [45–47] and an atomic force microscope (AFM) is most com-

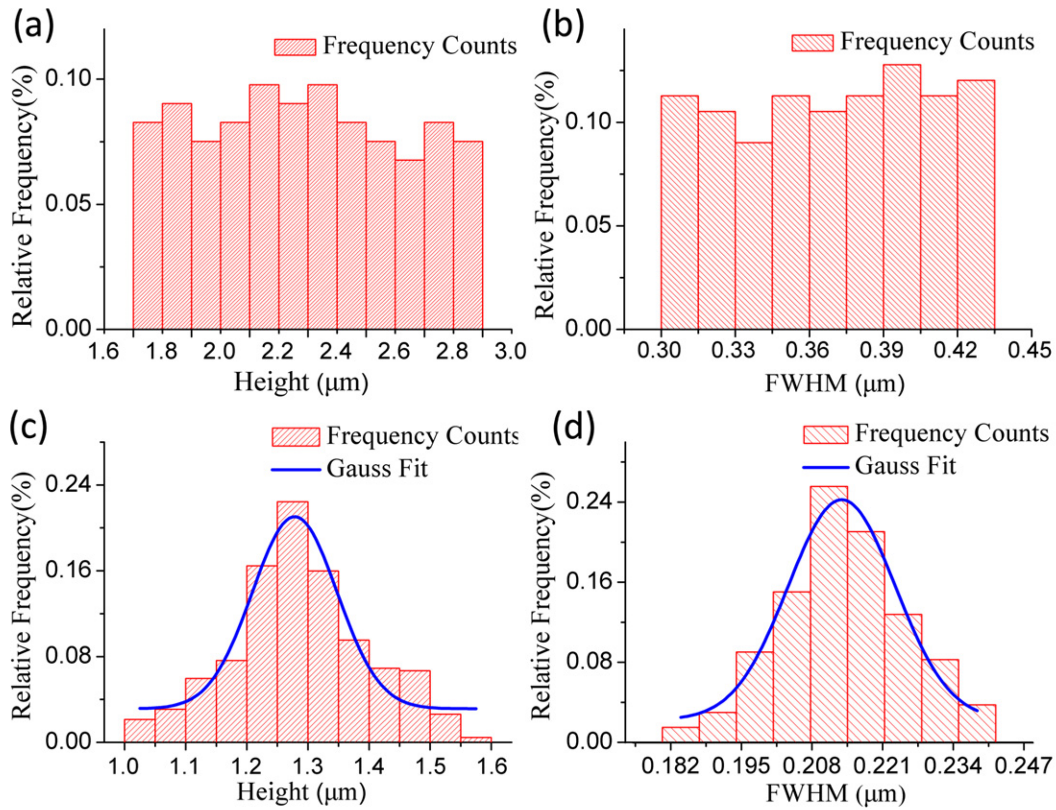

Figure 9. Frequency distribution histograms of shape parameters of black silicon sample I (a), (b) and II (c), (d). Reprinted with permission from [4]. Copyright 2013 IEEE.

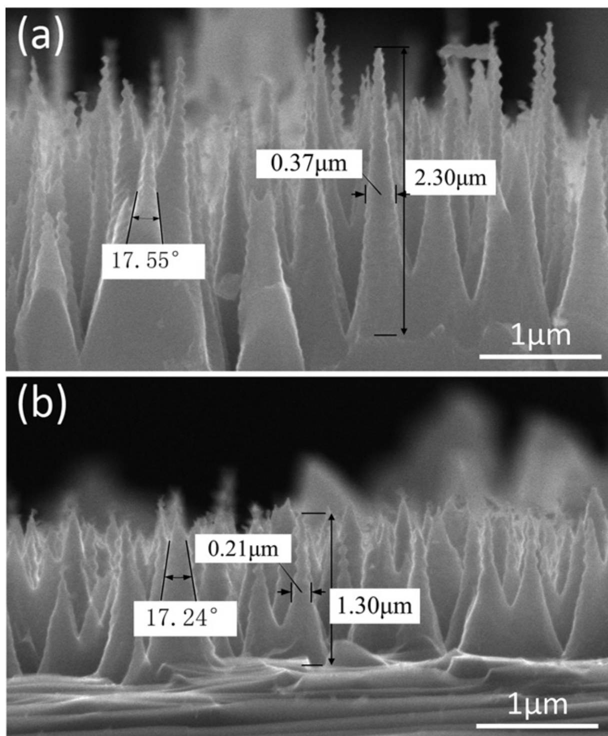

Figure 10. Illustration of result verification by manually measuring shape parameters of sample I (a) and II (b) by cross-sectional view SEM images. Reprinted with permission from [4]. Copyright 2013 IEEE.

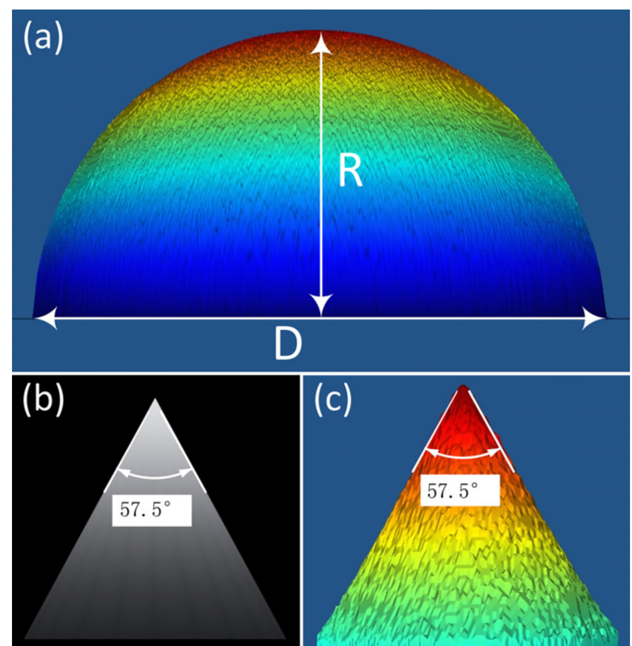

Figure 11. Verification of the reconstruction result of the synthetic sphere and cone in figure 7: front view of (a) reconstructed sphere, (b) original cone, (c) reconstructed cone.

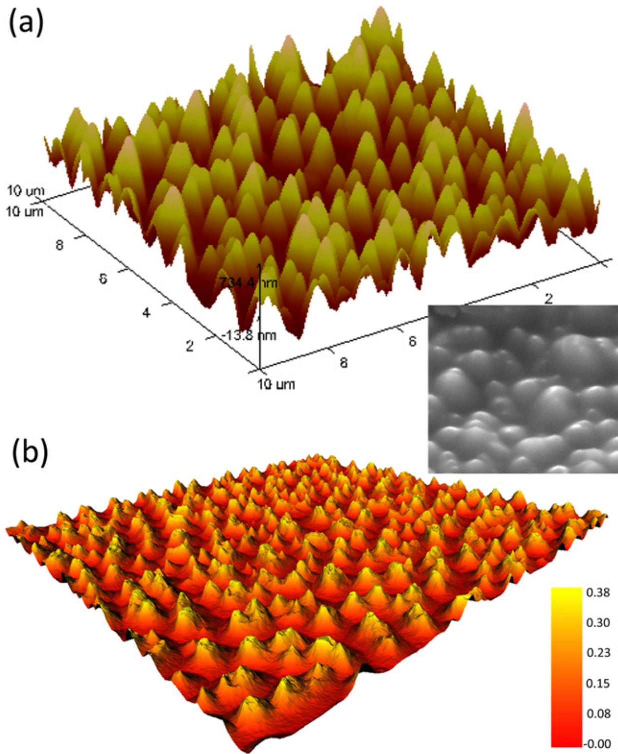

Figure 12. Roughness characterization by (a) AFM measurement and (b) 3D reconstruction method; inset: SEM image of the sample used in this experiment. Reprinted with permission from [4]. Copyright 2013 IEEE.

monly used to measure the roughness of micro/nano structures. The calculation method can be described as follows:

$$S_q = \sqrt{\frac{\sum (Z_i - Z_{\text{mean}})^2}{N}}. \tag{9}$$

Here, N is the number of measured height values, Z_i is the height value of number i, and Z_{mean} is the mean value of all the height values within the measured area.

According to the reconstruction results shown above, the root mean square (RMS) average of height deviations (i.e. roughness) of the sample can be calculated easily by equation (9) with the height values achieved by 3D reconstruction. As is shown in figure 12, the calculated roughness (RMS = 245 nm) is extremely close to the value measured by AFM ($S_q = 233$ nm). Another advantage of this method is that it has fewer limits for nanostructure shape and size, because the AFM cannot measure structures with very high aspect ratio and high density.

4.2. Optical property characterization of black silicon

Low reflectance is one of the main attractive properties of black silicon. Many fabrication methods have been utilized to achieve silicon surfaces with lower-reflective structures. This favorable property of black silicon strongly depends on the shape parameters of nanostructures. However, nanostructure morphology is not completely regular, and it takes a lot of time to measure the shape parameters and sometimes the values are inaccurate. With specific shape parameters of black silicon

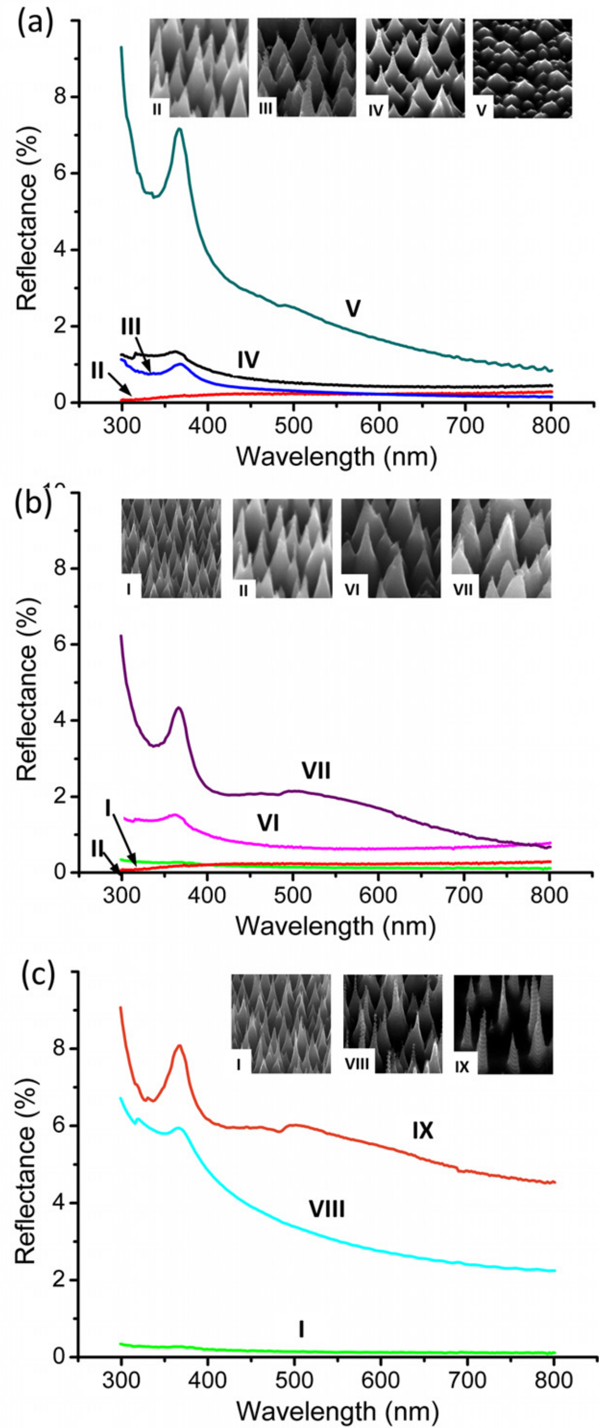

Figure 13. Reflectance of black silicon with respect to (a) aspect ratio, (b) height and (c) density, extracted by reconstruction. Reprinted with permission from [4]. Copyright 2013 IEEE.

extracted by 3D reconstruction, it is very easy to determine the influence of various nanostructures on optical properties. Reflectance (R) of nine samples I–IX with known texture parameters was measured in the visible range from 300 to 800 nm. From figure 13(a), it can be seen that reflectance declines ($R_{\text{V}} > R_{\text{IV}} > R_{\text{III}} > R_{\text{II}}$) as aspect ratio ($AR$) enlarges ($AR_{\text{V}} < AR_{\text{IV}} < AR_{\text{III}} < AR_{\text{II}}$) when their densities ($D$) are the same. In figure 13(b), the reflectance of the structures with the

same AR decreases more ($R_{\mathrm{I}} < R_{\mathrm{II}} < R_{\mathrm{VI}} < R_{\mathrm{VII}}$) with their heights ($h$) decreasing ($h_{\mathrm{I}} < h_{\mathrm{II}} < h_{\mathrm{VI}} < h_{\mathrm{VII}}$). If both AR and h are constant, larger density ($D_{\mathrm{I}} > D_{\mathrm{VIII}} > D_{\mathrm{IX}}$) will result in lower reflectance ($R_{\mathrm{I}} < R_{\mathrm{VIII}} < R_{\mathrm{IX}}$), as shown in figure 13(c).

Therefore, it can be concluded that in order to fabricate ultra-low reflective black silicon surfaces in the visible light region, aspect ratio and density should be enhanced and height should be reduced.

5. Conclusions

In summary, a 3D reconstruction method of nanostructures was put forward in this paper using only one top-view SEM image. According to the SEM imaging principle, contrast in an SEM image is determined by the generated amount of secondary electrons at every point on the surface, while the generation of secondary electrons is determined by the corresponding surface topography. By analyzing the gray-scale information of the SEM image through the SFS technique, the relationship between the contrast of the SEM image and the surface topography was established. After an equation solving process, it is simple to obtain both the 3D morphology of nanostructures and their detailed information. We took nanocone structures of black silicon samples and ideal sphere and cone structures as examples to investigate the quality, capability and efficiency of this 3D reconstruction method. The reconstruction results coincided well with the original structures, proving the rationality and validity of this method.

The main advantage of the method is the flexibility offered by SEM. Images of any region on samples can be obtained immediately in a non-destructive way, and the lateral and vertical resolutions can reach a very high level, because they are limited only by the quality of the acquired SEM images. Only one top-view SEM image is required as input. This is a great convenience in image preparation. Also, this method is fast, low-cost and highly efficient. It has been developed into commercial software, NanoViewer, which is user-friendly, succinct and effective, with a good display. However, this method still has some problems to be resolved. For example, the structure sidewall slope cannot be larger than 88°, otherwise there is no sidewall information kept in the SEM image, and the quality of SEM images can be affected by several factors when they are taken, which will influence the reconstruction result correspondingly. Further work will focus on the above problems and improvement of the accuracy of the method.

This 3D reconstruction method shows promise for use in a great many applications, such as analyzing surface roughness, offering data support for optimizing optical properties by studying the influence of nanostructure parameters, and so on. It also can be extended to check fabrication quality automatically in the mass production, packaging and testing of nanostructures. As 3D reconstruction by a single image has great application prospects, it is worthy of in-depth research. This paper has made a good start, and the results will be increasingly improved in the future.

Acknowledgments

The authors would like to thank the Key Laboratory for Physics and Chemistry of Nanodevices for their help with the operation of the scanning electron microscope. The authors also wish to thank the State Key Laboratory of Advanced Optical Communication Systems and Networks for the assistance in AFM measurement. This work is supported by the National Natural Science Foundation of China (Grant No. 91023045 and No. 61176103), National Key Laboratory Fund (9140C7901080902) and Doctoral Program Fund (No. 20110001110103).

References

[1] Demming A 2012 *Nanotechnology* **23** 250201
[2] Zhang X S, Han M D, Wang R X, Zhu F Y, Li Z H, Wang W and Zhang H X 2013 *Nano Lett.* **13** 1168–72
[3] Cai H, Dong B, Tao J F, Ding L, Tsai J M, Lo G Q, Liu A Q and Kwong D L 2013 *Appl. Phys. Lett.* **102** 023103
[4] Zhu F Y, Wang Q Q, Zhang X S, Hu W, Zhao X and Zhang H X 2013 *Int. Conf. on Solid-State Sensors, Actuators and Microsystems (Barcelona, June 2013)*
[5] Shulaker M M, Wei H, Patil N, Provine J, Chen H-Y, Wong H-S P and Mitra S 2011 *Nano Lett.* **11** 1881–6
[6] Brun T, Mercier D, Koumela A, Marcoux C and Duraffourg L 2012 *Appl. Phys. Lett.* **101** 183506
[7] Wang Z L 2009 *Mater. Sci. Eng.* R **64** 33–71
[8] Nguyen K N *et al* 2012 *Microsyst. Technol.* **18** 1807–14
[9] Fiala J C 2005 *J. Microsc.* **218** 52–61
[10] Uchic M D, Groeber M A, Dimiduk D M and Simmons J P 2006 *Scr. Mater.* **55** 23–8
[11] Villinger C, Gregorius H, Kranz C, Hohn K, Munzberg C, von Wichert G, Mizaikoff B, Wanner G and Walther P 2012 *Histochem. Cell Biol.* **138** 549–56
[12] Joos J, Carraro T, Weber A and Ivers-Tiffée E 2011 *J. Power Sources* **196** 7302–7
[13] Shahbazmohamadi S and Jordan E H 2012 *Meas. Sci. Technol.* **23** 125601
[14] Sequeira V, Ng K, Wolfart E, Gonçalves J G M and Hogg D 1998 *Proc. SPIE* **3641** 106–17
[15] Lee P H, Huang J W and Lin H Y 2012 *IEEE Int. Symp. on Intelligent Signal Processing and Communication Systems* pp 58–63
[16] Jordan E H, Gell M, Sohn Y H, Goberman D, Shaw L, Jiang S, Wang M, Xiao T D, Wang Y and Strutt P 2001 *Mater. Sci. Eng.* A **301** 80–9
[17] Stampfl J, Scherer S, Gruber M and Kolednik O 1996 *Appl. Phys.* A **63** 341–6
[18] Cho M and Javidi B 2009 *J. Disp. Technol.* **5** 345–9
[19] Marian A, Nada O, Légaré F, Meunier J, Vidal F, Roy S, Brunette I and Costantino S 2013 *J. Cataract. Refract. Surg.* **39** 118–27
[20] Tatschl A and Kolednik O 2003 *Mater. Sci. Eng.* A **356** 447–63
[21] Tatschl A and Kolednik O 2003 *Mater. Sci. Eng.* A **339** 265–80
[22] Musienko A, Tatschl A, Schmidegg K, Kolednik O, Pippan R and Cailletaud G 2007 *Acta Mater.* **55** 4121–36
[23] Marinello F, Bariani P, Savio E, Horsewell A and De Chiffre L 2008 *Meas. Sci. Technol.* **19** 065705
[24] Horn B K P 1970 *Doctoral Thesis* Cambridge
[25] O' Hara R and Barnes D 2012 *ISPRS J. Photogramm. Remote Sens.* **67** 27–34

[26] Wang G-H, Han J-Q and Zhang X-M 2009 *Meas. Sci. Technol.* **20** 125801

[27] Huang J, O'Sullivan F and Jike L 2012 *Inverse Problems* **28** 065009

[28] Czepkowski T and Slowko W 1996 *Scanning* **18** 433–46

[29] Drzazga W, Paluszynski J and Slowko W 2006 *Meas. Sci. Technol.* **17** 28–31

[30] Paluszynski J and Slowko W 2009 *J. Microsc.* **233** 10–7

[31] Paluszynski J and Slowko W 2005 *Vacuum* **78** 533–7

[32] Young R A and Kalin R V 1986 *Microelectronics processing: inorganic materials characterization (ACS Symp. Series) (Plymouth, USA)*

[33] Reimschuessel A C 1972 *J. Chem. Edu.* **49** A413–9

[34] Seiler H 1983 *J. Appl. Phys.* **54** R1–R18

[35] Avinun-Kalish M, Sagy O, Im S M, Lee C H, Oh J, Lim J, Kim C and Yoo H 2009 *Advanced Semiconductor Manufacturing Conf.* pp 223–7

[36] Anwar S, Smith L N and Smith M L 2012 *IJCSI Int. J. Comput. Sci. Issues* **9** 113–21

[37] Zhang R, Tsai P-S, Cryer J E and Shah M 1999 *IEEE Trans. Pattern Anal. Mach. Intell.* **21** 690–704

[38] Durou J-D, Falcone M and Sagona M 2008 *Comput. Vis. Image Underst.* **109** 22–43

[39] Intellisense Corporation 2013 (www.intellisense.com/newsview.aspx?id=18)

[40] Mehran M, Mohajerzadeh S, Sanaee Z and Abdi Y 2010 *Appl. Phys. Lett.* **96** 203101

[41] Sun G Y, Gao T L, Zhao X and Zhang H X 2010 *J. Micromech. Microeng.* **20** 075028

[42] Zhu F Y, Zhang X S, Hu W and Zhang H X *8th IEEE Int. Conf. on Nano/Micro Engineered and Molecular Systems (Suzhou, China, April 2013)*

[43] Zhang X S, Di Q L, Zhu F Y, Sun G Y and Zhang H X 2011 *Micro Nano Lett.* **6** 947–50

[44] Kalem S, Werner P, Arthursson O, Talalaev V, Nilsson B, Hagberg M, Frederiksen H and Sodervall U 2011 *Nanotechnology* **22** 235307

[45] Dong W P, Sullivan P J and Stout K J 1993 *Wear* **167** 9–21

[46] Dong W P and Stout K J 1995 *Wear* **181–183** 700–16

[47] Stout K J, Durakbasa M N and Osanna P H 2009 *Wear* **266** 511–4